Breathing with floating ribs: XROMM analysis of lung ventilation in savannah monitor lizards

Robert L. Cieri[1]*, Sabine Moritz[2], John G. Capano[3] and Elizabeth L. Brainerd[3]

1: Department of Biology, University of Utah, Salt Lake City, UT 84112, USA
2: Department of Biology, Community College of Rhode Island, Warwick, RI 02886, USA
3: Department of Ecology and Evolutionary Biology, Brown University, Providence, RI 02912, USA

*Author for correspondence (bob.cieri@gmail.com)

Key Words: Varanus, respiratory, trunk, Squamata, costal

Abstract

The structures and functions of the vertebrate lung and trunk are linked through the act of ventilation, but the connections between these structures and functions are poorly understood. We used XROMM to measure rib kinematics during lung ventilation in three savannah monitor lizards, *Varanus exanthematicus*. All of the dorsal ribs, including the floating ribs, contributed to ventilation; the magnitude and kinematic pattern showed no detectable cranial-to-caudal gradient. The true ribs acted as two rigid bodies connected by flexible cartilage, with the vertebral rib and ventromedial shaft of each sternal rib remaining rigid and the cartilage between them forming a flexible intracostal joint. Rib rotations can be decomposed into bucket handle rotation around a dorsoventral axis, pump handle rotation around a mediolateral axis, and caliper motion around a craniocaudal axis. Dorsal rib motion was dominated by roughly equal contributions of bucket and pump rotation in two individuals and by bucket rotation in the third individual. The recruitment of floating ribs during ventilation in monitors is strikingly different from the situation in iguanas, where only the first few true ribs contribute to breathing. This difference may be related to the design of the pulmonary system and life history traits in these two species. Motion of the floating ribs may maximize ventilation of the caudally and ventrolaterally-positioned compliant saccular chambers in the lungs of varanids, while restriction of ventilation to a few true ribs may maximize crypsis in iguanas.

Summary Statement

In savannah monitors, all dorsal ribs, both true and floating, contribute equally to ventilation, in contrast to green iguanas, where ventilation is dominated by the true ribs.

List of Abbreviations

XROMM: X-ray Reconstruction of Moving Morphology
savannah01-savannah03: Individual 1-3
kV: kilovolts
mA: milliamps
CT: Computed tomography
JCS: Joint coordinate system

Introduction

What is the relationship between the design of the lung and the trunk in vertebrates? Costal inspiration and expiration are likely the basal condition for amniotes (Brainerd and Owerkowicz, 2006), so it is reasonable to expect that amniote ribs are designed primarily to effect ventilation by moving to generate sub and super-atmospheric pressures in the thoracic cavity, and that the lung is designed primarily to be ventilated in this manner. Both structures, however, are affected by other parts of the body. The trunk functions in body support and locomotion, either by providing a stable chassis for motions of the limbs (Carrier, 1990; Carrier, 1993; Ritter, 1995; Ritter, 1996) or by generating locomotor work itself by lateral (Ritter, 1996) or dorsoventral (Carrier, 1996) oscillation. Lungs may also be ventilated by accessory trunk muscles such as diaphragms (Gans and Clark, 1976; Bramble and Jenkins, 1993; Farmer and Carrier, 2000), motion of the appendicular skeleton (Boggs et al., 1997; Boggs, 2002), cardiogenic oscillation (Szecwak and Jackson, 1992; Farmer, 2010), and gular pumping (Owerkowicz and Brainerd, 2006). The interactions between the design of the trunk and lung are therefore far from straightforward.

Squamates are a good group for investigating lung-trunk interactions because they lack accessory breathing mechanisms in their trunks, such as the diaphragm of mammals or

sternal pump of birds (Carrier, 1987; Claessens, 2009), and therefore rely primarily on costal movements for lung ventilation (Brainerd and Owerkowicz, 2006). Costal anatomy varies greatly among squamates, with species showing variable numbers of both true and floating ribs consisting of one to three different segments (Hoffstetter and Gasc, 1969). The axial skeleton in the trunk region of the savannah monitor (*Varanus exanthematicus*) consists of the vertebral column, with 28 presacral vertebrae, sternum, and between eighteen and twenty-two pairs of ribs (Cieri, 2018). The cranial-most four ribs are cervical ribs, followed by 18-22 dorsal ribs, starting with three true ribs with vertebral portions, hereafter referred to as vertebral ribs, connected directly to the sternum by sternal portions (Fig. 1D), hereafter referred to as sternal ribs. The remaining 11-15 ribs are floating ribs, with only a vertebral portion (Cieri, 2018). By comparison, green iguanas (*Iguana iguana*) possess 23 presacral vertebrae, four cervical ribs, four true ribs, four xiphisternal ribs, and nine floating ribs, of which the cranial four are considerably longer than the others (Carrier 1988; Brainerd et al., 2016).

Because squamates possess unicapitate ribs (Hoffstetter and Gasc, 1969), the rotations of these ribs at their costovertebral joints during any particular activity cannot be predicted *a priori* and must be measured empirically (Brainerd et al., 2016). The three-dimensional rotations of ribs can be decomposed into three components, which we will orient around the animal's main body axes *sensu* Brainerd et al. (2016): bucket handle rotation around a dorsoventral axis, caliper rotation around a cranio-caudal axis, and pump handle rotation around a mediolateral axis (Fig. 1).

Lung morphology in squamates is also quite diverse. Iguanas and varanids both exhibit unidirectional pulmonary airflow (Cieri et al., 2014; Schachner et al., 2013), but iguanas have comparatively simple bicameral lungs, whereas the lungs of varanids are multicameral, showing comparatively greater heterogeneity in compliance and in the distribution of gas-exchange parenchyma (Perry and Duncker, 1978, Perry and Duncker, 1980). An intrapulmonary bronchus runs through the lung, terminating in an abdominal sac-like bronchus, and gives rise to ten or more lateral bronchi, and a cervical bronchus (Schachner et al., 2013). In iguana lungs, a powerful jet of air during inspiration moves

air caudad in the lateral portion and craniad in the medial portion of the larger, ventral chamber during both phases of ventilation (Cieri et al., 2014). Similarly, air moves craniad between the successive caudal, lateral chambers during both inspiration and expiration in the lungs of varanids (Schachner et al., 2013). The relationship between the manner in which these two types of lungs are ventilated and pattern of air flow within them remains unexplored.

The overall pattern of rib motion within the trunk of *I. iguana* and *V. exanthematicus* is qualitatively different. Ventilation in *I. iguana* is restricted to the first few true ribs (Brainerd et al., 2016), whereas all the true ribs plus most of the floating ribs (Fig. 1) appear to move during ventilation in *V. exanthematicus* (Owerkowicz et al, 1999). Comparison of detailed ventilatory kinematics in these two species is a practical first step to investigating how iguanas and varanids can ventilate their lungs effectively and generate unidirectional airflow using qualitatively different patterns of rib motions.

A previous XROMM (X-ray reconstruction of moving morphology) investigation into ventilation in *I. iguana* found motion of the vertebral ribs to be dominated by bucket handle rotation (Brainerd et al., 2016). How does the motion of the true ribs differ in varanids, and how does the motion of the floating ribs differ from the true ribs? We conducted an XROMM analysis to answer these questions by measuring the rotations of the true and floating ribs during ventilation in savannah monitors.

Materials and Methods

Three savannah monitors of roughly similar body mass were used in this study: savannah01, 1.4 kg; savannah02, 1.2 kg; and savannah03, 0.95 kg. All animal care and experimental procedures were approved by the Institutional Animal Care and Use Committee of Brown University. X-ray video and CT scan data collected and analyzed for this study are available from the X-ray Motion Analysis Portal (xmaportal.org) in Study ID BROWN42. Video data are stored and documented with metadata in

accordance with best practices for video data management in organismal biology (Brainerd et al., 2017).

Both marker-based (Brainerd et al., 2010) and markerless (Gatesy et al., 2010) XROMM techniques (methodological details in referenced papers) were used in this study in order to create 3D animations of the vertebral column, ribs and sternum. For marker-based XROMM, at least three radiopaque, tantalum markers were implanted in each bone of interest to facilitate automatic software tracking of high-contrast points. The lizards were placed under isoflurane anesthesia, and holes were drilled into the ribs and sterna with an 0.25 or 0.8 mm diameter hand drill. Ribs were marked with 'beads-on-posts': 1 mm tantalum beads (Baltec, Los Angeles, CA, USA) with holes laser-drilled into them, mounted on short (2-3 mm long) segments of 000 size (0.25 mm diameter) insect pins. The sternum was marked with 0.8 mm solid tantalum beads (Baltec, Los Angeles, CA, USA). Beads and posts were manually press-fitted into the holes. Vertebrae were marked with conical tungsten carbide markers (Kambic et al., 2014). The lizards recovered from surgical procedures for a minimum of three days before data recording began. Analgesics were administered before and after surgery. All individuals resumed normal behavior and feeding within three days.

X-Ray videos were collected on custom-made biplanar videoradiography equipment (Miranda et al., 2011) at the Keck Lab at Brown University. Videos were recorded at 60-100 frames per second using between 50-75 kV and 200 mA of radiation. Breaths were recorded from unrestrained animals placed in large plastic enclosures roughly twice the size of the XROMM field of view.

Eight deep breaths were analyzed from savannah01, six from savannah02, and five from savannah03. These breaths were collected after a gas mixture containing between 10-20% carbon dioxide 80-90% and atmospheric air was circulated through the enclosures. Other breaths, including shallower breaths and breaths with a highly curved posture of the spine were recorded but not analyzed as part of this study. Deep breaths were analyzed originally to enable comparisons with previous work in *I. iguana,* and because maximal

breaths would presumably be of similar tidal volume.

CT scans of the trunks of each animal were collected before and after bead implantation with an Animage Fidex veterinary CT scanner (Fidex, Animage, Pleasanton, CA, USA). Isotropic voxel sizes were 0.15 or 0.3 mm. Polygonal mesh surface models of the marked bones and metal markers were created in Horos (Purview, Annapolis, MD, USA; www.horosproject.org).

X-ray videos were processed using XMALab (Knorlein et al., 2016) to create rigid body transformations for marker-based XROMM and undistorted video sequences for Scientific Rotoscoping (Brainerd et al., 2010; Gatesy et al., 2010). Rigid-body coordinates were calculated and filtered with a low-pass Butterworth filter in XMALab (cut-off frequency 1 Hz) and then used to animate bone surface models segmented from CT scans in Maya animation software (Autodesk, San Rafael, CA, USA). For markerless Scientific Rotoscoping, bones models were manually aligned with undistorted x-ray video sequences in Maya.

For each individual, animations of the vertebrae and first two dorsal ribs were generated from marker-based XROMM, and the motion of the sternum was generated from a combination of markerless and marker-based XROMM, where the sternum's translation was constrained by the motion of a single bead and its rotation was animated using Scientific Rotoscoping. The marker-based technique was used to animate each sternal rib from the motion of two beads and a virtual marker digitally locked to the sternum at the relevant sternocostal joint. Analysis of fully marked sterna and sternal ribs determined that little to no translation occurs at these sternocostal joints. Thus we were able to use the center of rotation about these joints as a fixed position relative to both sternum and sternal ribs. This virtual point was then locked to the sternum and acted as an additional rigid-body point to animate the associated sternal ribs.

Pure markerless XROMM (Scientific Rotoscoping) was employed to generate animations of unmarked ribs in two individuals: savannah01, the third vertebral, and second, fourth,

and sixth floating ribs; and savannah02, the third vertebral rib, as well as the second, fourth, sixth, and eighth floating ribs. In addition, the second floating rib of savannah03 was marked with three beads and animated using marker-based XROMM. We chose to mark the anterior ribs because these are the ribs that contributed substantially to ventilation in *I. Iguana* (Brainerd et al., 2016). Due to the long time investment inherent in scientific rotoscoping, only a few breaths per animal were animated for this initial investigation. The final skeletal animations made using scientific rotoscoping each have between five and seven animation handles that had to be individually and manually manipulated to align the animation bones with the dorsal and lateral x-ray projections and generate smooth and accurate motions.

Joint coordinate systems (JCS) were established in Maya to quantify the relative translation and rotations of bones occurring in each XROMM animation. To facilitate meaningful comparisons between different breaths in different individuals, the zero points for each JCS were defined at an artificial position where each rib formed a 90-degree angle with its proximal attachment, representing an exaggerated inspiration (Brainerd et al., 2016). These JCSs were established at the costovertebral and sternocostal joints. To facilitate comparison with previously published data on *I. iguana* (Brainerd et al., 2016), the Z-axis was oriented dorsoventrally to capture bucket handle rotation. Polarity is established by the right-hand rule, such that exhalation is associated with decreasing or more negative bucket handle angles, and inspiration is associated with increasing or more positive bucket handle angles (Fig. 2). Zero caliper motion was set artificially from a pose where the proximal portion of each dorsal rib was positioned parallel to the coronal plane running through its respective vertebral centrum or sternum.

To quantify differences in posture of the sternum observed during different breaths, a vertebral-sternal JCS was established where the vertebral column and sternum are parallel at the zero position. In this JCS, the Z-axis corresponds to rotation in the sagittal plane, such that rotation of the cranial aspect of the sternum towards the vertebral column maps to a higher JCS rotation angle. The same JCS was used to measure translations of the sternum relative to the vertebral column, to determine whether there is some

dorsoventral collapse of the thorax during exhalation. This vertebral-sternal JCS was also applied to the *I. iguana* dataset (Brainerd et al., 2016) to measure dorsoventral collapse for comparison.

To make meaningful comparisons between breaths that differed in size and duration, rotations were scaled around each mean component angle and scaled to total breath duration. To compare the relative contribution of each form of rotation between animals and breaths, the total rotation angles were summed to form a total rotation value, and the contributions of bucket, caliper, and pump rotations were expressed as percentages.

In order to validate the accuracy of the rotoscoping method, the fifth rib from savannah03 was animated in five trials using both marker-based and Scientific Rotoscoping techniques (Supplementary Fig. S1). The mean Euler angles during each breath did not differ between animation methods in x, y, or z (Wilcoxon test, $p=0.31$ (x), $p=0.69$ (y), $p=0.55$ (z)), nor did the total amount of rotation (Wilcoxon test, $p=0.10$) or the total range of pump (Wilcoxon test, $p=0.10$), caliper (Wilcoxon test, $p=0.31$) or bucket (Wilcoxon test, $p=0.84$) motion.

The precision of marker tracking *in vivo* can be estimated by the relative motion of pairs of markers in a rigid bone (Brainerd et al., 2010; Dawson et al., 2011; Tashman and Anderst, 2003). Small errors in marker tracking will manifest as noise around the relative distance signal, which is expected to be zero between two markers in a rigid body (Figure 3) and can be quantified by the standard deviation of intermarker distance in rigid bones. In this study, this marker tracking error ranged from 0.03 to 0.27 mm with an average of 0.062 mm. All statistical tests were completed in RStudio (version 1.1.456).

Results

To determine how to animate the motion of skeletal elements, it was first necessary to determine which elements functioned as rigid bodies during the breath cycle. To this end, we analyzed the distance between markers along one true rib during the breath cycle (Fig. 3). Pairwise distances between markers within the vertebral ribs do not change measurably during the breath, indicating that the vertebral ribs move as rigid bodies. Markers placed in the thin, curved dorsolateral aspect of the sternal ribs, however, move relative to markers in the main shaft of the same sternal rib, which do not move relative to each other, indicating that only the main shaft of the sternal ribs behaves as a rigid body. Furthermore, the dorsolateralmost sternal rib marker does not move relative to markers in the dorsal rib portions, so the dorsolateralmost aspect of the sternal rib portions can be considered part of the vertebral portion's rigid body. Although beads in the dorsal tip of each sternal rib often moved with the vertebral rib, vertebral rib motion was animated using only the beads implanted in the vertebral rib itself, and sternal rib to sternum motion was reconstructed using only the two ventral beads in the sternal rib and a virtual point parented to the sternum at its point of articulation with the sternal rib.

Neutral breathing rib and sternum positions differed between individuals. The sternum was held significantly more parallel to the vertebral column in savannah03 than in savannah01 or savannah02 ($p<0.05$ Tukey post-hoc comparison). The resting posture of the first vertebral rib also differed between individuals with a significantly higher resting pump handle angle in savannah03. Resting bucket handle and caliper angles were significantly higher and lower, respectively, in savannah01 than savannah02 or savannah03. The resting posture of the sternal portion of the first true rib also differed between individuals with savannah01 having a significantly lower resting pump handle angle than savannah02, a significantly higher resting caliper angle than either savannah02 or savannah03, and a significantly higher resting bucket handle rotation angle than either savannah02 or savannah03 (all $p<0.05$, Tukey-Kramer post-hoc pairwise comparisons).

During all but one breath analyzed (Table S3), the sternum and vertebral column translated towards each other during expiration and apart during inspiration along a dorsoventral axis with an average magnitude of 3.41 mm (s.d. = 2.43). The magnitude of this motion was not appreciably different between standing vs. prone breaths but was slightly higher in savannah01 (4.60 ± 1.72 mm) compared to savannah02 (2.52 ± 2.26 mm) or savannah03 (2.60 ± 3.20 mm). By comparison, this motion was 1.08 ± 0.6 mm in *I. iguana,* measured from the prior iguana dataset (Brainerd *et al.,* 2016).

3D Costal Kinematics During Ventilation

Marker-baser animations of the vertebral elements of the first two dorsal ribs reveal a breathing pattern exhibiting small amounts of caliper motion and variable amounts of pump handle and bucket handle motion. Breaths from savannah02 were dominated by pump handle motion (Table 1, Fig. 4), and bucket handle motion dominated breaths from savannah03 in the first dorsal rib (Table 1). Breaths from savannah01 represented an intermediate between the extremes of the other animals (Fig. 5). Breaths from savannah02 consisted of significantly more pump handle motion than savannah03 ($p<0.001$, Nemenyi post hoc comparisons following Kruskal-Wallace tests).

In all animals, the first and second vertebral rib rotated caudad during exhalation and the distal rib tip moved caudad and dorsad, collapsing the rib cage and effecting a volume reduction of the thorax. Caliper motion caused the distal tip of the vertebral rib to rotate mediad during exhalation, further contributing to rib cage collapse and thoracic volume reduction.

Motion of the sternal ribs involved all three types of rotation around the sternum, with caliper rotation the least dominant component (Fig. 5B and Table 1). During a typical breath from savannah02 (Fig. 4), the sternal ribs moved caudad and craniad during expiration and inspiration, respectively, similar to the vertebral ribs. During peak expiration the sternal rib also rotated dorsally using caliper motion to remain in contact with the ventral tip of the vertebral rib, which translated dorsally due to the pump handle

motion of the vertebral rib. This motion is necessary because the sternal rib exhibits greater bucket handle rotation than the vertebral rib, with the main sternal rib shaft moving further caudad than the main dorsal rib shaft during peak exhalation. Rotation angles for the true ribs are provided in Supplementary Table S1.

As the sternum and vertebral column translated towards each other along a dorsoventral axis during expiration and away from each other during inspiration, the vertebral and sternal ribs rotate relative to each other along their broad cartilaginous connections. As the rib cage collapses during expiration the angle formed on the cranial side of the vertebral and sternal ribs in the sagittal plane becomes more acute (Movie S2). In addition, the proximal angle between the vertebral and sternal ribs in the transverse plane decrease as the rib cage collapses. Both of these motions serve to decrease the thoracic volume and effect expiration.

Pump handle motion contributed relatively less to vertebral rib motion in savannah03 compared to savannah01 and savannah02 and this animal's dorsal ribs centered around a swept back posture with a high resting pump angle. In contrast, pump handle was the dominant motion in savannah02, and this animal's ribs moved around a more inflated posture with a lower resting pump angle. Differences in resting posture, however, provides an incomplete explanation for differences in ventilatory kinematics; savannah01 had the lowest resting pump angle but the contribution of pump angle motion to total ventilation in this animal was intermediate between savannah02 and savannah03.

Motion of Floating Ribs

It is evident from qualitative observation of the x-ray videos that the vertebral segments of all of the dorsal ribs, both true and floating, participate in ventilation in all individuals (Fig. 6, Movie 1, Movie 3). In savannah01 (Fig. 7) and savannah02, the total degrees of rotation across all components did not differ between different sets of ribs (Kruskal-Wallace test), and in savannah03 the second floating rib, i.e. the fifth dorsal rib, rotated more than the vertebral ribs of the first or second dorsal ribs ($p<0.05$, Wilcoxon rank sum

test). Raw rotation angles for the floating ribs are provided in Supplementary Table S2. The middle ribs (F2-6 in Fig. 7) appear to rotate more than the cranial and caudal ribs, but a higher sample size is necessary to determine whether this pattern is typical of *V. exanthematicus*.

Discussion

The most striking finding of this investigation is that the motions of the floating ribs of *V. exanthematicus* during ventilation are similar to those of the vertebral elements of the true ribs, both in magnitude and kinematic pattern. This is surprising because we expected rib kinematics to be at least somewhat powered by muscular and skeletal connections to the sternal ribs (DeTroyer, 2005), and thus that the floating ribs would move less or differently from the vertebral elements of the true ribs. Perhaps the sternal elements of the true ribs follow the lead of their vertebral elements in *V. exanthematicus*, or the soft tissues of the rib cage link the motions of the vertebral and floating ribs together into a uniform pattern, similar to their role during hooding in cobras (Young and Kardong, 2010).

This extensive use of floating ribs for ventilation is unlike the situation in iguanas. In *I. iguana,* only the ribs that bear sternal connections move substantially during breathing, and a caudal gradient of decreasing bucket handle rotation is observed (Brainerd et al., 2016). Iguanas seem to maintain a more rigid thorax in general during breathing and locomotion compared to varanids, an observation that may explain these differences. The average dorsoventral expansion and collapse of the trunk during a breath, accomplished by the motion of the sternum relative to the vertebral column, is greater in *V. exanthematicus* compared to two individuals of *I. iguana* of greater body mass. *I. iguana* is an arboreal herbivore and relies on crypsis to avoid predation (Greene et al., 1978). Reducing the overall motion of the body during breathing by confining of the ventilatory motion to a few cranial ribs and limiting dorsoventral compression may help them breathe without being spotted by predators.

Electromyography of the hypaxial musculature during ventilation in *I. iguana* found that external and internal intercostal muscles were the only muscles to be active during inspiration (Carrier, 1989), and that only the anterior sections of these muscles, between the first few ribs, were active. If the intercostals are also responsible for inspiration in *V. exanthematicus,* the increased number of ribs participating in ventilation is likely due to simultaneous activity of all of the intercostal muscles, as seen during locomotion in *I. iguana* (Carrier, 1990). If *V. exanthematicus* also uses all of the intercostals during locomotion, which seems likely because both species use similar forms of locomotion, this condition raises two interesting possibilities. First, because the relative amount of ventilatory motion is more equal along the entire rib cage in varanids than iguanas, varanids may be better able than iguanas to harness the motion of the trunk during locomotion to ventilate their lungs while moving, better avoiding Carrier's constraint (Carrier, 1987) at low to moderate speeds (Wang et al., 1997). This, along with differences in exercised-induced circulatory impairment (Farmer and Hicks, 2000; Munns et al., 2004) and gular pumping in varanids (Owerkowicz et al., 1999, Owerkowicz et al., 2001), may help to explain the why varanids show higher locomotor stamina than iguanas (Wang et al., 1997). XROMM analysis of rib motion and electromyographical recordings of muscle activity during locomotion are needed to clarify the role of the hypaxial musculature in varanids. Furthermore, the possible role of body motion on the movement of air through the lungs, from one lung to another, and from the atmosphere to the lung needs to be examined.

The relative importance of floating rib motion between *V. exanthematicus* and *I. iguana* may be related to the design of the lung in each animal. Although varanid lizards and iguanas both have unidirectional pulmonary airflow (Schachner et al., 2013, Cieri et al., 2014, Cieri and Farmer, 2016), they have dissimilar lung structures. The lungs of *I. iguana* have two large, semi-partitioned chambers joined by openings close to the entrance of the trachea (Cieri et al., 2014) without a well-developed intrapulmonary bronchus. By comparison, varanid lungs are multicameral, consisting of a dense, gas-

exchanging center surrounded by compliant, saclike chambers running along an intrapulmonary bronchus. The compliant chambers are most developed along the caudal and ventrolateral aspects (Milani, 1984; Wolf, 1933; Kirschfeld, 1970; Becker et al., 1989; Schachner et al., 2013), and have been hypothesized to serve as a bellows, responsible for ventilating the parenchymal region (Wolf, 1933; Perry, 1998; Klein and Owerkowicz, 2006**)**. If this hypothesis is correct, the expansion and contraction of the caudal trunk due to motion of the floating ribs may be necessary to achieve optimal ventilation of the gas exchange region of the lung. Although the situation in *I. iguana* demonstrates that this anatomical arrangement is not necessary for unidirectional pulmonary airflow *sensu stricto* (Cieri et al., 2014; Farmer, 2015a; Farmer, 2015b; Cieri and Farmer, 2016), comparatively large distensions of these sac-like chambers may maximize ventilation of the gas exchanging tissue in the lungs of varanids.

Another important finding is that the kinematic pattern of ribs during ventilation in *Varanus,* consisting of both pump and bucket handle rotation, is qualitatively and quantitatively different from that observed in *I. iguana,* which uses bucket handle rotation almost exclusively (Brainerd et al., 2016). Varanid lizards possess a post pulmonary septum (Duncker, 1978), the tensioning of which during inspiration may be important to enable full expansion of the caudal, compliant lung chambers (Klein and Owerkowicz, 2006). The movement of floating ribs reported here during inspiration may be critical to a full lung inspiration in *Varanus,* but would be of limited importance in *Iguana,* which lacks a post pulmonary septum. Because the post pulmonary septum attaches to the body wall laterally close to the distal floating rip tips (Klein and Owerkowicz, 2006), pump handle rotation of these ribs might be important to completely tension this septum during inspiration. If pump handle rotation in the dorsal ribs is important in tensioning post pulmonary membranes, pump handle rotation should be found in *Teiioidea* and *Chameleonidae*, which possess post-hepatic and post-pulmonary septa, respectively (Klein and Owerkowicz, 2006). Capano *et al.,* (2017), however, found ventilation in *Salvator merianae*, the Argentine black and white tegu (*Teiiodiea*), to be dominated by bucket rotation. Teiids have smooth muscle in the central portion of their post-hepatic septum (Klein and Owerkowicz, 2006), contraction of which may be sufficient to fully

tension the septum without pump handle motion of the ribs. On the other hand, complete tensioning of the post-hepatic septum may be less critical to Teiids, which have unicameral lungs, compared to varanids, which have multicameral lungs with the most compliant regions are located ventrolaterally.

The increased pump handle motion observed in *V. exanthematicus* compared to *I. iguana* and *S. merianae* may instead be a biomechanical consequence of differences in the trunk designs of these three species. Compared to *I. iguana* and *S. merianae, V. exanthematicus* has more floating (*I.i., 9; S.m.,* 5; *V.e.*, 13) and fewer true ribs (*I.i.* 4 true, 4 xiphisternal*; S.m.* 3 true, 3 xiphisternal*; V.e*. 3 true, 0 xiphisternal) (Carrier, 1988; Cieri, 2018; Brainerd et al., 2016; Hoffstetter and Gasc, 1969). The motion of a vertebral element of a true rib, as opposed to a floating rib, should be constrained to bucket rotation by its connection to the sternum because pump handle motion would naturally either pull the sternal rib dorsally, dislocate the dorsal from the sternal rib, or force the sternal rib to bend in order to prevent this dislocation. In contrast, a floating rib, subject to no sternal restrictions, is comparatively freer to rotate along a lateral axis. Pump motion in the true, dorsal ribs of *V. exanthematicus* can also be explained by this mechanism - pump motion of the floating ribs will cause pump motion in the true ribs as well, due to the muscular linkages consisting of the internal and external intercostals (Cieri, 2018) running between each successive rib (Young and Kardong, 2010).

The observed differences in rib kinematics may also be related to differences in the muscular anatomies of *I. iguana* and *V. exanthematicus.* Carrier (1988) reports ligaments connecting the ribs of *I. iguana* to the vertebrae that restrict motion of the ribs in all but a cranial or caudal direction, but these ligaments are not present in *V. exanthematicus* (Cieri, 2018) and it is possible to rotate the dorsal ribs in all three planes. Electromyography of the hypaxial muscles during ventilation in iguanas shows that the external and internal intercostals are active during inspiration while the *retrahentes costarum* and *transversalis* are active during expiration.

Inspiration in *V. exanthematicus* may be powered not only by the internal and external intercostals, which could act to pull the ribs together, causing bucket handle motion, but also *supracostalis dorsus brevis* (Cieri, 2018), which inserts on each dorsal rib and is poised to generate positive caliper and positive pump handle motion of the dorsal rib. The relative activity of this muscle versus the intercostals could potentially explain the variation in the contributions of bucket and pump handle rotations seen between individuals among the dorsal ribs in this study. For exhalation, *retrahentes costarum* in *I. iguana* originates from the ventral aspect of the vertebral centrae and inserts on the mid-portion of the vertebral ribs (Carrier, 1989), with a line of action poised to cause negative bucket handle rotation of the vertebral ribs. On the other hand, the thoracic portion of *transversalis* originates on the mid-portion of the vertebral portion of the true ribs and inserts onto the sternal ribs (Carrier, 1989) and would instead cause pump handle and caliper rotation. Because *V. exanthematicus* does not have *retrahentes costarum* but does have *transversalis* (Cieri, 2018), contraction of the *transversalis* by itself during exhalation could cause the positive pump handle rotation during exhalation seen in this study (Figs 4 and 5).

The rib kinematics measured in this study are diverse between but remarkably consistent within individuals. The diminished dorsal rib pump handle motion seen in savannah03 could be related to the fact that all breaths from this animal were recorded while the animal was prone. There are no differences, however, in the relative contribution of pump and bucket motion between standing and prone breaths from savannah01 or savannah02. It is possible that savannah monitors may use different ventilatory kinematics under different conditions such as after large meals, while gravid, after exercise, or during breaths at different tidal volumes, as well as during different life-history stages. Future work analyzing breaths under different conditions and body postures may provide additional information about the full kinematic flexibility of the lepidosaur trunk.

Concluding remarks

The findings of this study help to illuminate the evolutionary linkages between ecology, axial anatomy, ventilation and the design of the pulmonary system in squamates. The effect of different ventilatory motions on pulmonary airflow patterns is unclear and warrants further investigation. The results of this work can be used to design kinematically-accurate boundary conditions for dynamic computational fluid dynamics simulations to test explicit hypotheses about the effect of regional ventilation on patterns of pulmonary airflow.

Acknowledgements

The authors are indebted to A. Camp, R. Carney, T. Dial, and E. Tavares for assistance with surgeries, data collection, and animal husbandry. The authors also thank D. Carrier and C.G. Farmer for discussions that greatly improved the manuscript.

This material is based upon work supported by the National Science Foundation Graduate Research Fellowship Program under Grant No. (1256065). Any opinions, findings, and conclusions or recommendations expressed in this material are those of the authors and do not necessarily reflect the views of the National Science Foundation.

Competing Interests

The authors declare no competing interests.

Funding

This work was funded by NSF grants 1120967, 1655756 and 1661129 to ELB and an NSF Graduate Research Fellowship to RC (Grant No. 1256065).

Data Availability

Data available on XMAPortal.org in the study "Monitor Lizard Breathing and Locomotion" with unique study ID BROWN42.

References

Becker, H.-O., Böhme, W. and Perry, S. F. (1989). Die Lungenmorphologie der Warane (Reptilia: Varanidae) und ihre systematisch-stammesgeschichtliche Bedeutung. *Bonner Zool. Beiträge* **40**, 27–56.

Bennet, D. (1994). Varanus exanthematicus. In *Varanoid Lizards of the World* (ed. Pianka, E. R. and King, D. R.), pp. 95–103. Bloomington, IN: Indiana University Press.

Boggs, D. F., Jenkins, F. A. and Dial, K. (1997). The effects of the wingbeat cycle on respiration in black-billed magpies (Pica pica). *J. Exp. Biol.* **200**, 1403–12.

Boggs, D. F. (2002). Interactions between locomotion and ventilation in tetrapods. *Comp. Biochem. Physiol. A. Mol. Integr. Physiol.* **133**, 269–88.

Bramble, D. M. and Jenkins, F. A. (1993). Mammalian locomotor-respiratory integration: implications for diaphragmatic and pulmonary design. *Science* **262**, 235–40.

Brainerd, E. L., Baier, D. B., Gatesy, S. M., Hedrick, T. L., Metzger, K. A., Gilbert, S. L. and Crisco, J. J. (2010). X-ray reconstruction of moving morphology (XROMM): precision, accuracy and applications in comparative biomechanics research. *J. Exp. Zool. A. Ecol. Genet. Physiol.* **313**, 262–79.

Brainerd, E.L., Blob, R.W., Hedrick, T.L., Creamer, A.T. and Müller, U.K. (2017). Data management rubric for video data in organismal biology. *Int. Comp. Biol.*, **57**, 33-47.

Brainerd, E. L., Moritz, S. and Ritter, D. A. (2016). XROMM analysis of rib kinematics during lung ventilation in the green iguana, *Iguana iguana*. *J. Exp. Biol.* **219**, 404–411.

Brainerd, E. L. and Owerkowicz, T. (2006). Functional morphology and evolution of aspiration breathing in tetrapods. *Respir. Physiol. Neurobiol.* **154**, 73–88.

Capano, J.G., Moritz, S. and Brainerd, E.L. (2017). Comparison of 3D rib kinematics during breathing in the Argentine black and white tegu, *Salvator merianae*, and green iguana, *Iguana iguana*. *Int. Comp. Biol.,* 57: E218.

Carrier, D. R. (1987). The evolution of locomotor stamina in tetrapods: circumventing a mechanical constraint. *Paleobiology* **13**, 326–341.

Carrier, D. R. (1988). Locomotor-ventilatory coupling in lizards and early tetrapods. *PhD thesis,* University of Michigan, Ann Arbor, MI.

Carrier, D. R. (1989). Ventilatory action of the hypaxial muscles of the lizard *Iguana iguana*: a function of slow muscle. *J. Exp. Biol.* **457**, 435–457.

Carrier, D. R. (1990). Activity of the hypaxial muscles during walking in the lizard *Iguana iguana*. *J. Exp. Biol.* **152**, 453–70.

Carrier, D. R. (1993). Action of the hypaxial muscles during walking and swimming in the salamander *Dicamptodon ensatus*. *J. Exp. Biol.* **83**, 75–83.

Carrier, D. R. (1996). Function of the intercostal muscles in trotting dogs: ventilation or locomotion? *J. Exp. Biol.* **199**, 1455–65.

Cieri, R.L. (2018). The axial anatomy of monitor lizards (*Varanidae*). Journal of Anatomy. doi:10.1111/joa.12872.

Cieri, R. L. and Farmer, C. G. (2016). Unidirectional pulmonary airflow in vertebrates: a review of structure, function, and evolution. *J. Comp. Physiol. B* **186**, 541–552.

Cieri, R. L., Craven, B. A., Schachner, E. R. and Farmer, C. G. (2014). New insight into the evolution of the vertebrate respiratory system and the discovery of unidirectional airflow in iguana lungs. *Proc. Natl. Acad. Sci.* **111**, 17218–17223.

Cieri, R. L. and Farmer, C. G. (2016). Unidirectional pulmonary airflow in vertebrates: a review of structure, function, and evolution. *J. Comp. Physiol. B* **186**, 541–552.

Claessens, L. P. a M. (2009). The skeletal kinematics of lung ventilation in three basal bird taxa (emu, tinamou, and guinea fowl). *J. Exp. Zool. A. Ecol. Genet. Physiol.* **311**, 586–99.

Dawson, M. M., Metzger, K. A, Baier, D. B. and Brainerd, E. L. (2011). Kinematics of the quadrate bone during feeding in mallard ducks. *J. Exp. Biol.* **214**, 2036–46.

De Troyer, A. (2005). Respiratory Action of the Intercostal Muscles. *Physiol. Rev.* **85**, 717–756.

Duncker, H. R. (1978). Coelom-Gliederung der Wirbeltiere-Funktionelle Aspekte. *Verh. Anat. Ges*. **72**, 91-112.

Farmer, C. G. (2010). The provenance of alveolar and parabronchial lungs: insights from paleoecology and the discovery of cardiogenic, unidirectional airflow in the American alligator (*Alligator mississippiensis*). *Physiol. Biochem. Zool.* **83**, 561–75.

Farmer, C. G. (2015). The evolution of unidirectional pulmonary airflow. *Physiology* **30**, 260–272.

Farmer, C. G. (2015). Unidirectional flow in lizard lungs: a paradigm shift in our understanding of lung evolution in Diapsida. *Zoology* **188**, 299–301.

Farmer, C. G. and Carrier, D. R. (2000). Pelvic aspiration in the American alligator (*Alligator mississippiensis*). *J. Exp. Biol.* **203**, 1679–87.

Farmer, C. G. and Hicks, J. W. (2000). Circulatory impairment induced by exercise in the lizard *Iguana iguana*. *J. Exp. Biol.* **203**, 2691–7.

Gans, C. and Clark, B. (1976). Studies on ventilation of caiman crocodilus (Crocodilia: Reptilia). *Respir. Physiol.* **26**, 285–301.

Gatesy, S. M., Baier, D. B., Jenkins, F. A. and Dial, K. P. (2010). Scientific rotoscoping: a morphology-based method of 3-D motion analysis and visualization. *J. Exp. Zool. A. Ecol. Genet. Physiol.* **313**, 244–61.

Greene, H. W., Burghardt, G. M., Dugan, B. A. and Rand, A. S. (1978). Predation and the defensive behavior of green iguanas (Reptilia, Lacertilia, Iguanidae). *J. Herpetol.* **12**, 169–176.

Hoffstetter, R. and Gasc, J. (1969). Vertebrae and Ribs of Modern Reptiles. In *Biology of the Reptilia V1* (ed. Gans, C.), pp. 201–310. London: Academic Press.

Kambic, R. E., Roberts, T. J. and Gatesy, S. M. (2014). Long-axis rotation: a missing degree of freedom in avian bipedal locomotion. *J. Exp. Biol.* **217**, 2770–2782.

Kirschfeld, U. (1970). Eine Bauplanalyse der Waranlunge. *Zool. Beitraege NF* **16**, 401–440.

Klein, W. and Owerkowicz, T. (2006). Function of intracoelomic septa in lung ventilation of amniotes: lessons from lizards. *Physiol. Biochem. Zool.* **79**, 1019–32.

Knörlein, B. J., Baier, D. B., Gatesy, S. M., Laurence-Chasen, J. D. and Brainerd, E. L. (2016). Validation of XMALab software for marker-based XROMM. *J. Exp. Biol.* jeb.145383.

Milani, A. (1894). Beiträge zur Kenntniss der Reptilienlunge. I. Lacertilia. *Zool. Jahrbucher* **10**, 93–146.

Miranda, D. L., Schwartz, J. B., Loomis, A. C., Brainerd, E. L., Fleming, B. C. and Crisco, J. J. (2011). Static and dynamic error of a biplanar videoradiography system using marker-based and markerless tracking techniques. *J. Biomech. Eng.* **133**, 121002.

Munns, S. L., Hartzler, L. K., Bennett, A. F. and Hicks, J. W. (2004). Elevated intra-abdominal pressure limits venous return during exercise in *Varanus exanthematicus*. *J. Exp. Biol.* **207**, 4111–20.

Owerkowicz, T., Brainerd, E. L. and Carrier, D. R. (2001). Electromyographic pattern of the gular pump in monitor lizards. *Bull. Mus. Comp. Zool* **156**, 237–248.

Owerkowicz, T., Farmer, C. G., Hicks, J. W. and Brainerd, E. L. (1999). Contribution of gular pumping to lung ventilation in monitor lizards. *Science* **284**, 1661–3.

Perry, S. F. and Duncker, H.-R. (1978). Lung architecture, volume and static mechanics in five species of lizards. *Respir. Physiol.* **34**, 61–81.

Perry, S. F. and Duncker, H. R. (1980). Interrelationship of static mechanical factors and anatomical structure in lung evolution. *J. Comp. Physiol. B* **138**, 321–334.

Perry, S. F. (1998). Lungs: Comparative Anatomy, Functional Morphology, and Evolution. In *Biology of the Reptilia Vol 19*, pp. 1–92. Society for the Study of Amphibians and Reptiles.

Ritter, D. (1995). Epaxial muscle function during locomotion in a lizard (*Varanus salvator*) and the proposal of a key innovation in the vertebrate axial musculoskeletal system. *J. Exp. Biol.* **198**, 2477–90.

Ritter, D. (1996). Axial muscle function during lizard locomotion. *J. Exp. Biol.* **199**, 2499–510.

Schachner, E. R., Cieri, R. L., Butler, J. P. and Farmer, C. G. (2013). Unidirectional pulmonary airflow patterns in the savannah monitor lizard. *Nature* **506**, 367–370.

Tashman, S. and Anderst, W. (2003). In-vivo measurement of dynamic joint motion using high speed biplane radiography and CT: application to canine ACL deficiency. *J Biomech Eng* **125**, 238–245.

Wang, T., Carrier, D. R. and Hicks, J. W. (1997). Ventilation and gas exchange in lizards during treadmill exercise. *J. Exp. Biol.* **200**, 2629–39.

Wolf, S. (1933). Zur kenntnis von bau und funktion der reptilienlunge. *Zollogische Jahrbucher* **57**, 139–190.

Young, B. A. and Kardong, K. V. (2010). The functional morphology of hooding in cobras. *J. Exp. Biol.* **213**, 1521–1528.

Tables

Table 1: Relative contribution of each rotation component to overall motion of the first vertebral and sternal rib for eight, six, and five breaths in savannah01-3, respectively.

Vertebral Rib 1	**savannah01 (%) n=8**	**savannah02 (%) n=6**	**savannah03 (%) n=5**
Pump	36.1 ± 6.59	58.54 ± 6.87*	13.97 ± 2.11
Caliper	11.9 ± 4.06	13.6 ± 4.43	10.02 ± 4.17
Bucket	51.9 ± 7.54	27.8 ± 7.32	76.0 ± 4.11
Sternal Rib 1			
Long-Axis	41.1 ± 8.45	36.5 ± 4.84	34.8 ± 1.44
Caliper	6.54 ± 2.54	10.43 ± 3.32	9.42 ± 1.87
Bucket	52.4 ± 6.38	53.1 ± 6.93	55.8 ± 1.08

* indicates statistically significant increase in pump handle composition compared to savannah 03

Table 2: Relative magnitude* of rotations of dorsal ribs during four, three, and five breaths in savannah01-3, respectively.

Rib	savannah01(%) n=4	savannah02(%) n=3	savannah03(%) n=5
V1	73.65	72.88	80.62
V2	59.85	82.19	82.31
V3	87.72	100	
F2	100	88.51	100
F4	75.18	89.70	
F6	76.64	74.48	
F8		54.03	

*Relative magnitudes of all rotations summed are expressed as a percentage of the rib with the greatest summed rotation. Absolute mean values (in degrees) for all rotations are found in Table S1.

Figures

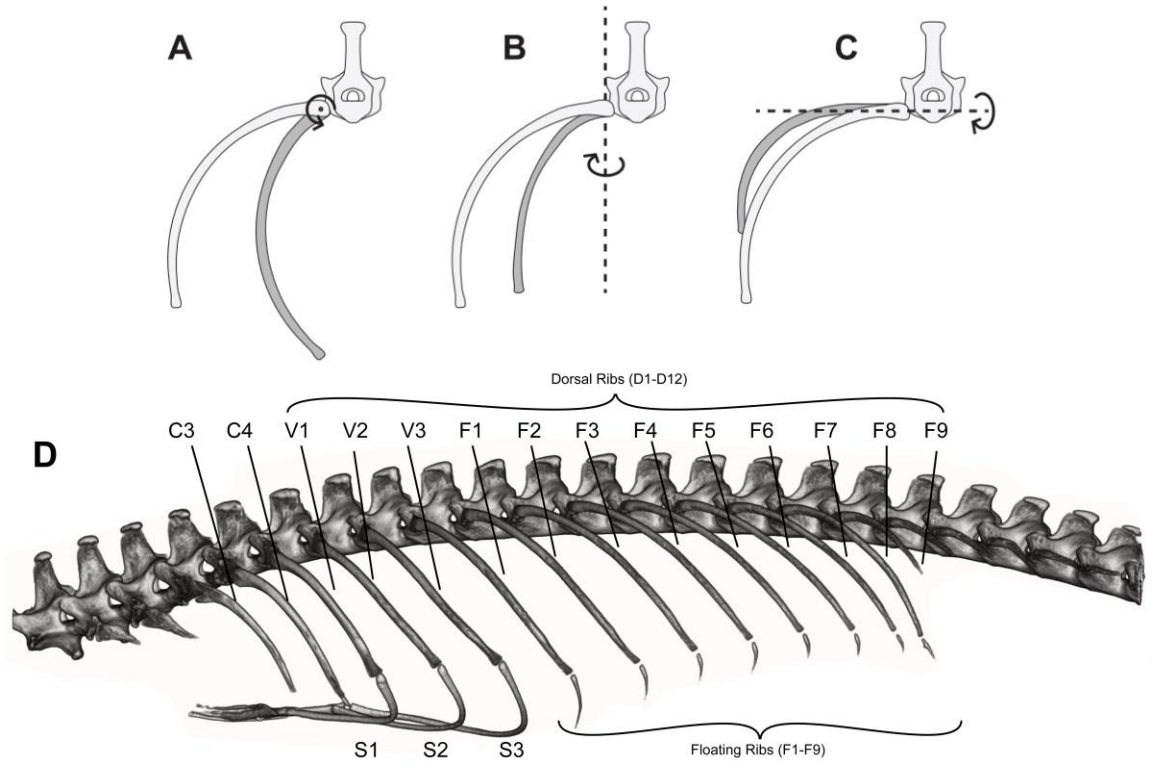

Fig. 1. Costal joint motion and axial anatomy in *V. exanthematicus.* Costal rotations can be described as a combination of three rotations: (A) caliper rotation around a craniocaudal axis, (B) bucket handle rotation around a dorsoventral axis, and (C) pump handle rotation around a mediolateral axis. The axial skeleton of *Varanus exanthematicus* (D) consists of the vertebral column, with 28 presacral vertebrae, sternum, and 18-22 pairs of ribs. There are four cervical ribs (C1-4), followed by dorsal ribs (D1-12) which include three true ribs with vertebral (V1-3) and sternal portions (S1-3) and a variable number of floating ribs (F1-9). Adapted from Cieri (2018).

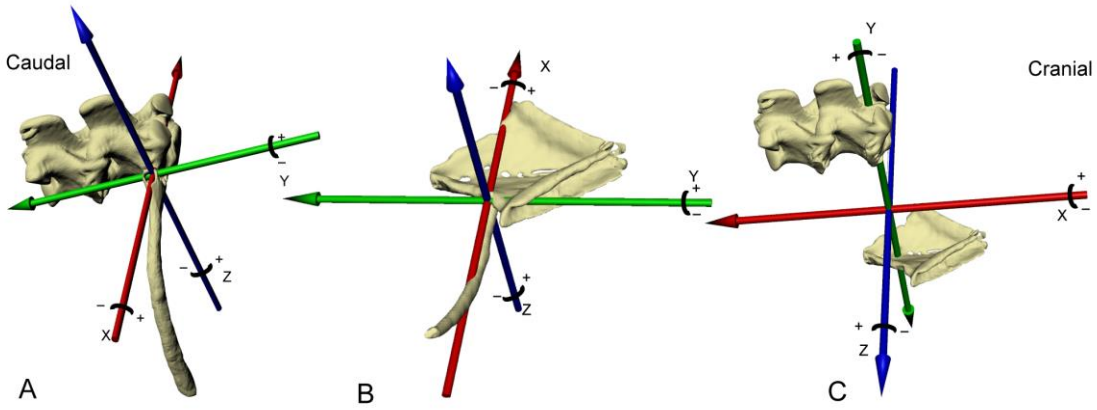

Fig. 2. Costovertebral, Sternocostal, and Vertebral-sternal joint coordinate systems. **(**A) The costovertebral joint coordinate system was used to quantify translation and rotation of the vertebral and floating ribs relative to the vertebral column. (B) The sternocostal joint coordinate system was used to quantify translation and rotation of the sternal ribs relative to the sternum. The system was established such that the X axis (red) records pump handle motion (also sometimes called long-axis rotation (Brainerd et al., 2016)), the Y axis (green) records caliper rotation, and the Z axis (blue) records bucket handle rotation. Polarity of the rotations is determined by the right-hand rule, and in each trial, the zero position for each rotation was set to an artificial but reproducible posture where the dorsal ribs and vertebral column formed a right angle, and the sternal ribs formed a right angle with the cranio-caudal body axis, representing an exaggerated full inspiration. (C) The vertebral-sternal joint coordinate system was used to quantify translation and rotation of the sternum relative to the vertebral column as an index of changes in body posture. The zero position for each rotation was set to an artificial but reproducible posture where the vertebral column and sternum were exactly parallel and occupied the same sagittal and coronal planes.

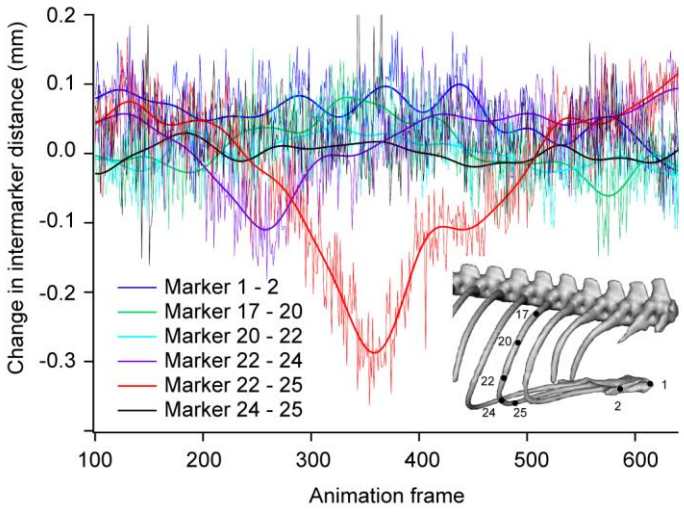

Fig. 3. Relative motion of vertebral and sternal rib segments during a representative breath in *V. exanthematicus*. Raw and filtered inter-marker distance traces are shown for savannah02. Beads 17-20, 22, and 24-25 correspond to the vertebral rib, the thin segment of the sternal rib, and the main shaft of the sternal rib, respectively.

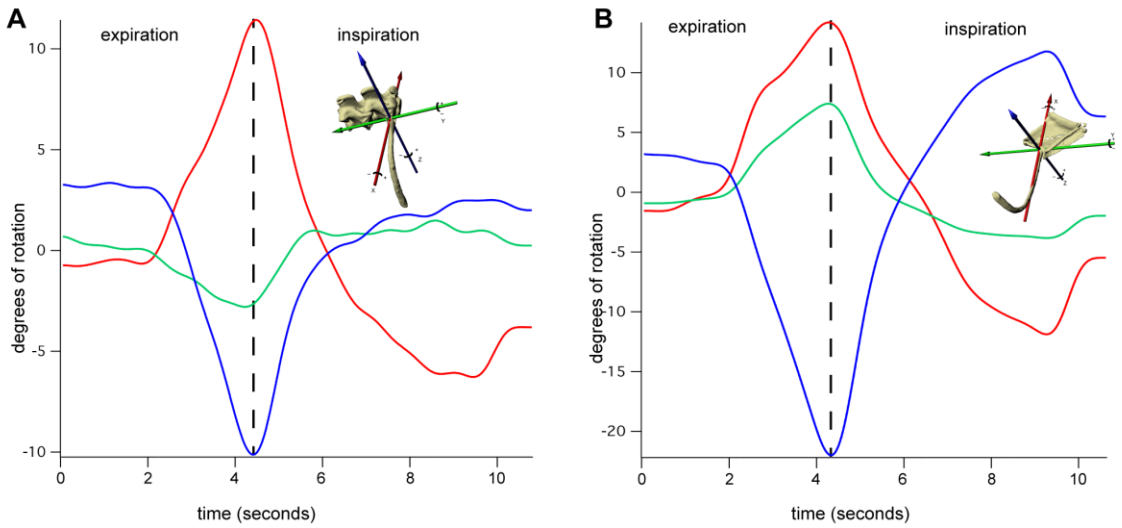

Fig. 4. Euler rotations at the costovertebral and sternocostal joints of the first dorsal rib. (A) costovertebral joint coordinate system (explained in Figure 2) and rotations of the first vertebral rib around its own articulation with the vertebral column during one deep breath from one individual (savannah02). The red trace depicts X axis pump handle motion, green Y axis caliper rotation, and the blue trace Z axis bucket handle motion. (B) sternocostal joint coordinate system and rotations of the first sternal rib around its own articulation with the sternum.

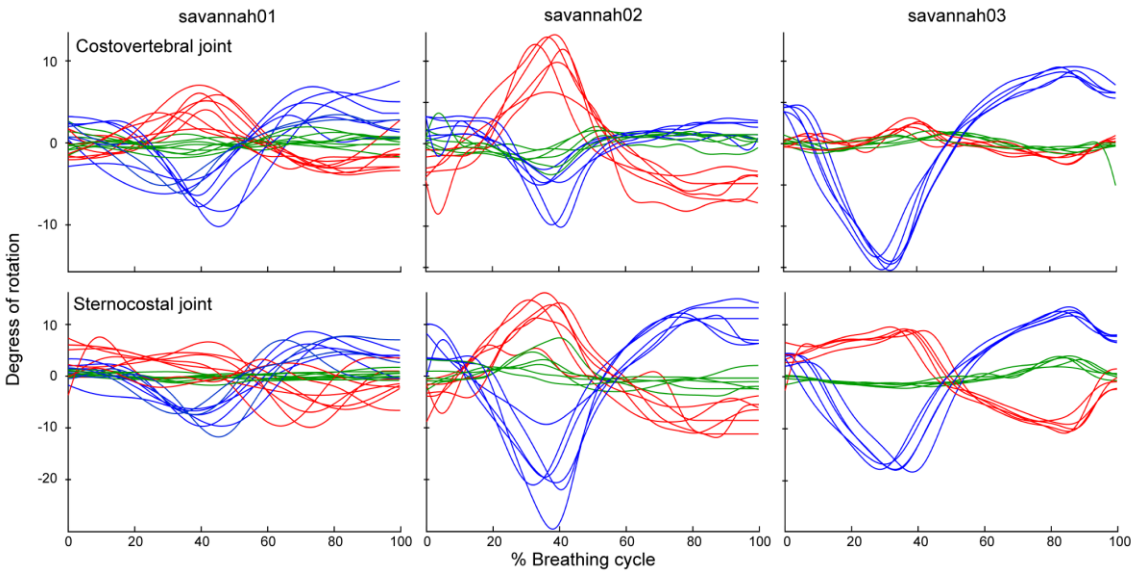

Fig. 5. Euler rotations of the first vertebral and sternal rib for all analyzed breaths in each individual. Each breath (savannah01, n=8; savannah02, n=6; savannah03, n=5) consists of an exhalation followed by an inspiration with rotation angles zeroed around their average and scaled to 100%. See materials section for details on each JCS. Costovertebral joint: red – pump handle rotation, green – caliper motion, blue – bucket handle rotation. Sternocostal joint: red – pump handle rotation, green – caliper motion, blue – bucket handle rotation.

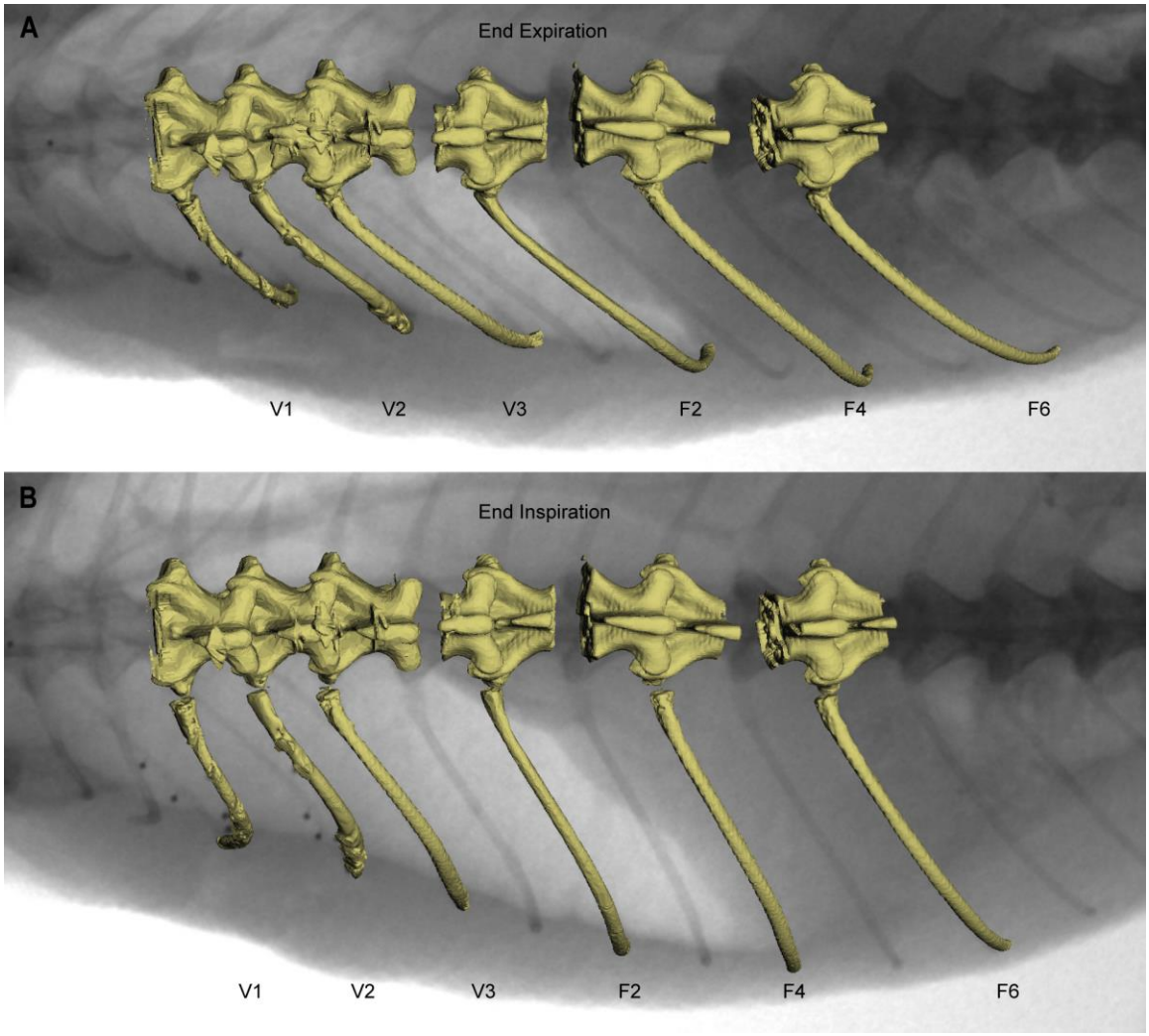

Fig. 6. Kinematics of floating ribs in a typical breath. Qualitative analysis of rib rotations during ventilation indicate that the floating ribs contribute to ventilation in *V. exanthematicus.* Markerless animation of caudal floating ribs (F2-6) at end expiration (A) and end inspiration (B) shows that these ribs show similar amounts of pump and bucket rotation to the vertebral segments of the cranial, true ribs (V1-3).

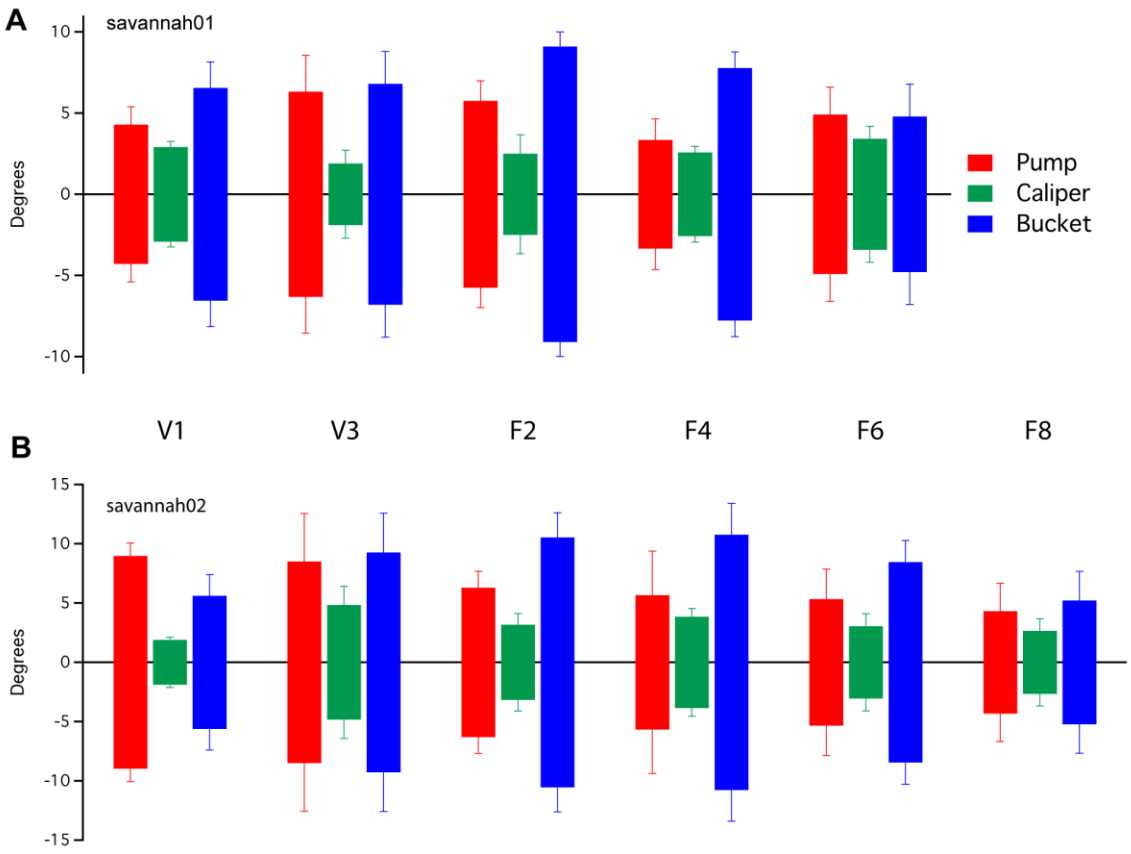

Fig. 7. Relative contribution of rib rotations in floating and true ribs. The mean total breath range (the angle of maximum exhalation subtracted from the angle of maximum inspiration) of pump handle (red), caliper (green), and bucket (blue) handle rotations centered around their mean values for true and floating ribs among all analyzed breaths in (A) savannah01 (n=4) and (B) savannah02 (n=3). Error bars show one standard deviation from the mean. No change in rib kinematics along a cranial to caudal gradient exists although overall motion is slightly reduced in magnitude by floating rib 9.

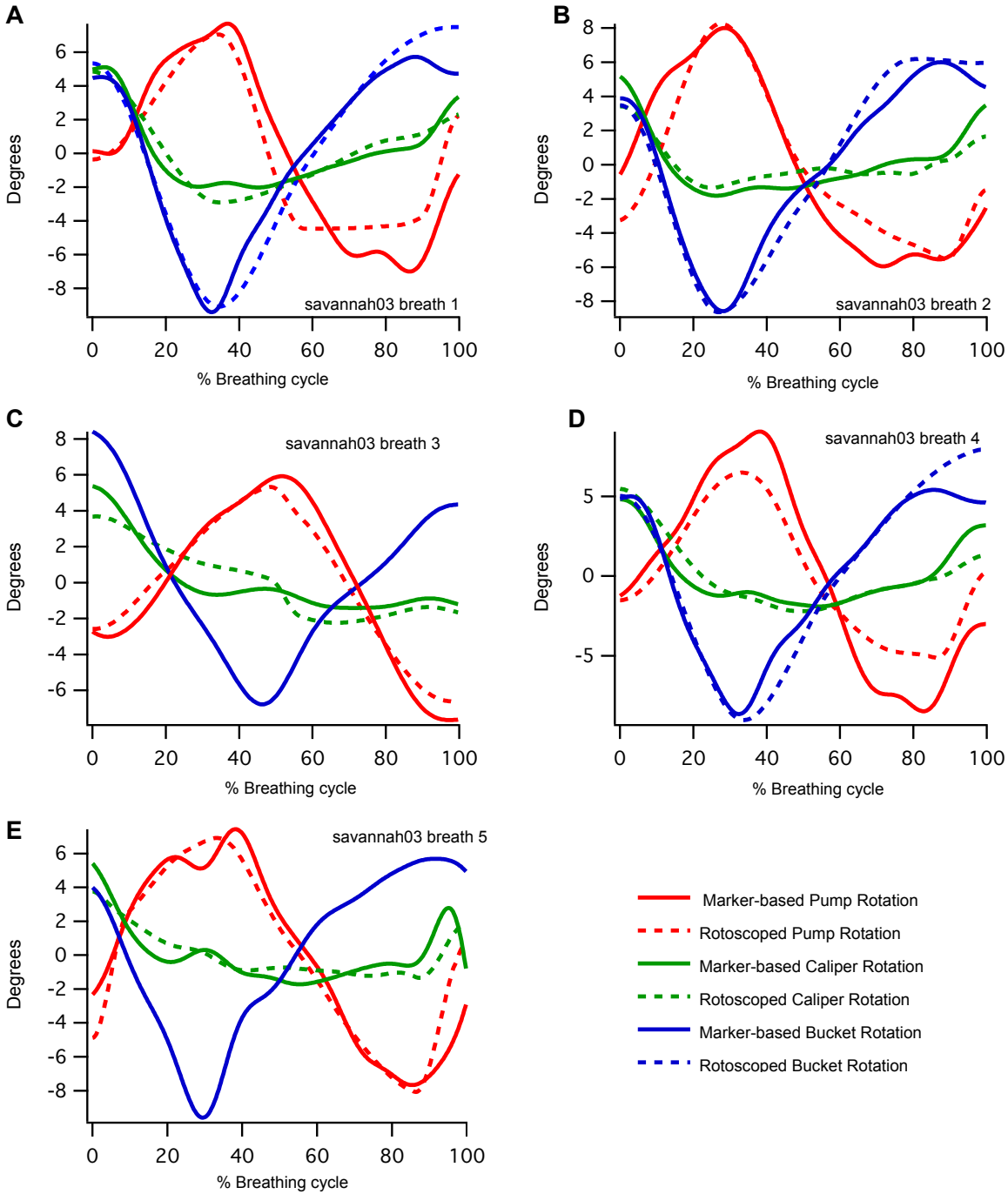

Fig. S1. Validation of rotoscoping. Comparison of kinematics of the third floating rib in savannah03 animated using the marker-based method (solid lines) and markerless Scientific Rotoscoping (dashed lines). Pump handle (red), caliper (green), and bucket handle (blue) rotations are centered around their average values and scaled to total breath duration. Five breaths are depicted.

Table S1: Rotations in degrees of vertebral ribs 1 and 2 (V1, V2) and sternal ribs 1 and 2 (S1 and S2) at the costovertebral joints and sternocostal joints, respectively for savannah01 (n=8), savannah02 (n=6), and savannah03 (n=5).

		V1			**V2**			**S1**			**S2**	
		sav01	sav02	sav03	sav01	sav02	sav03	sav01	sav02	sav03	sav02	sav03
Z Bucket[1]												
max Inhale	mean	-32.4	-20.0	-13.9	-35.6	-1.5	-3.6	-42.4	-45.9	-59.6	-23.1	-22.2
	s.d.	6.1	6.6	1.2	3.7	11.7	0.7	4.1	5.6	2.0	24.8	25.9
max Exhale	mean	-44.1	-28.7	-37.4	-44.4	-9.4	-8.4	-57.1	-78.7	-89.9	-40.5	-30.1
	s.d.	7.8	6.5	1.8	5.5	13.4	2.1	4.6	4.6	2.2	37.9	36.5
magnitude[2]	mean	11.7	8.7	23.5	8.7	7.8	4.9	11.9	22.3	30.3	17.3	7.9
	s.d.	3.1	3.8	1.0	2.7	2.3	2.1	3.7	3.9	0.6	14.6	10.7
Y Caliper[1]												
max Inhale	mean	-0.12	-5.7	-6.5	0.7	15.8	47.7	10.3	0.86	3.7	26.2	57.0
	s.d.	4.3	3.6	1.7	2.7	7.9	2.3	6.0	6.8	2.2	26.1	38.2
max Exhale	mean	-2.8	-9.8	-9.7	-1.4	1.7	39.4	8.4	-5.6	-1.4	10.7	42.1
	s.d.	4.2	2.3	1.9	2.5	2.4	2.1	6.2	7.3	1.3	19.1	31.8
magnitude[2]	mean	2.6	4.1	3.2	2.1	14.1	8.4	1.8	6.4	5.1	15.5	14.9
	sd	0.9	1.7	1.7	1.2	7.2	1.5	0.8	2.6	1.1	10.8	7.6
X Pump[1]												
max Inhale	mean	10.5	27.3	35.5	0.8	13.7	0.1	7.6	46.1	26.2	24.3	14.8
	s.d.	6.3	3.1	2.7	2.4	14.9	0.2	6.4	8.4	5.0	27.8	32.9
max Exhale	mean	2.5	9.8	31.1	-6.0	2.7	-0.5	-4.4	23.8	7.3	14.6	10.7
	s.d.	7.6	3.1	2.0	3.1	4.6	0.5	9.5	8.6	4.6	16.7	23.9
magnitude[2]	mean	8.0	17.6	4.4	6.8	10.9	0.6	14.8	32.8	18.9	10.0	4.1
	s.d.	1.8	3.3	0.9	2.1	12.2	0.6	2.8	7.7	0.8	11.3	9.0

[1]rotation axes are defined by the JCS in Fig. 2.
[2]magnitude is defined as the difference in degrees between maximum exhale and maximum inhale.

Table S2: Rotations in degrees of vertebral rib 3 and floating ribs 2, 4, 6, and 8 (V3, F2, F4, F6, F8) at the costovertebral joints for savannah01 (n=4), savannah02 (n=3), and savannah03 (n=5).

		V3		**F2**			**F4**		**F6**		**F8**
		sav01	sav02	sav01	sav02	sav03	sav01	sav02	sav01	sav02	sav02
Z Bucket[1]											
max Inhale	mean	-47.97	-19.85	-37.88	-11.67	-30.08	-30.46	-22.18	-18.60	-19.45	-35.57
	s.d.	6.74	4.35	8.06	11.36	1.42	7.28	4.87	9.77	21.55	24.97
max Exhale	mean	-61.56	-38.40	-56.07	-32.77	-44.93	-45.99	-43.72	-28.16	-36.36	-46.03
	s.d.	2.98	10.07	9.12	12.45	1.74	9.25	6.09	10.55	20.13	28.53
magnitude[2]	mean	13.60	18.55	18.19	21.09	14.85	15.53	21.54	9.56	16.91	1.46
	s.d.	4.00	6.61	1.79	4.14	0.52	2.00	5.28	3.99	3.64	4.86
Y Caliper[1]											
max Inhale	mean	-14.53	-3.36	-8.56	-4.80	-1.70	-8.51	-9.98	-0.06	-17.08	-10.79
	s.d.	4.14	6.37	2.74	5.65	2.25	8.03	4.35	6.65	5.11	4.32
max Exhale	mean	-18.32	-16.04	-13.49	-11.16	-10.04	-12.99	-17.69	-6.88	-23.20	-16.12
	s.d.	2.52	7.57	0.99	5.44	1.81	7.84	5.23	5.25	7.17	4.14
magnitude[2]	mean	3.79	9.68	4.93	6.65	8.34	4.49	7.71	6.83	6.11	5.33
	s.d.	1.63	3.17	2.42	1.86	3.00	0.70	1.36	1.54	2.09	2.02
X Pump[1]											
max Inhale	mean	15.30	35.89	13.51	22.77	22.89	8.25	23.11	20.23	25.84	21.87
	s.d.	6.01	2.34	4.74	5.58	4.52	7.68	14.82	10.32	12.37	5.88
max Exhale	mean	2.69	18.87	2.43	10.17	7.60	2.56	11.77	10.40	15.16	13.21
	s.d.	3.76	5.79	2.62	3.76	4.36	7.36	7.57	9.78	10.18	5.00
magnitude[2]	mean	12.61	17.02	11.08	12.61	15.29	5.69	11.34	9.82	10.68	8.66
	s.d.	4.48	8.09	2.32	2.76	2.23	2.59	7.41	3.36	5.04	4.69

[1]rotation axes are defined by the JCS in Fig. 2.
[2]magnitude is defined as the difference in degrees between maximum exhale and maximum inhale.

Table S3: Range of vertical displacement (mm) between the sternum and vertebral column measured by the vertebral-sternal JCSs during breaths in *Iguana iguana*[1] and *Varanus exanthematicus*[2].

	Breath 1	**Breath 2**	**Breath 3**	**Breath 4**	**Breath 5**	**Breath 6**	**Breath 7**	**Breath 8**
Iguana02	0.66	01.36	0.556	0.586	0.97			
Iguana05	1.14	0.90	2.51					
Iguana mean		1.08 ± 0.64						
Savannah01	2.29	4.89	4.98	06.57	4.86	4.69	1.90	6.59
Savannah02	1.91	1.05	2.33	1.70	7.03	1.13		
Savannah03	1.00	1.43	8.30	1.07	1.17			
Varanid mean		3.41 ± 2.43						

1: Brainerd et al., 2016; 2: This study

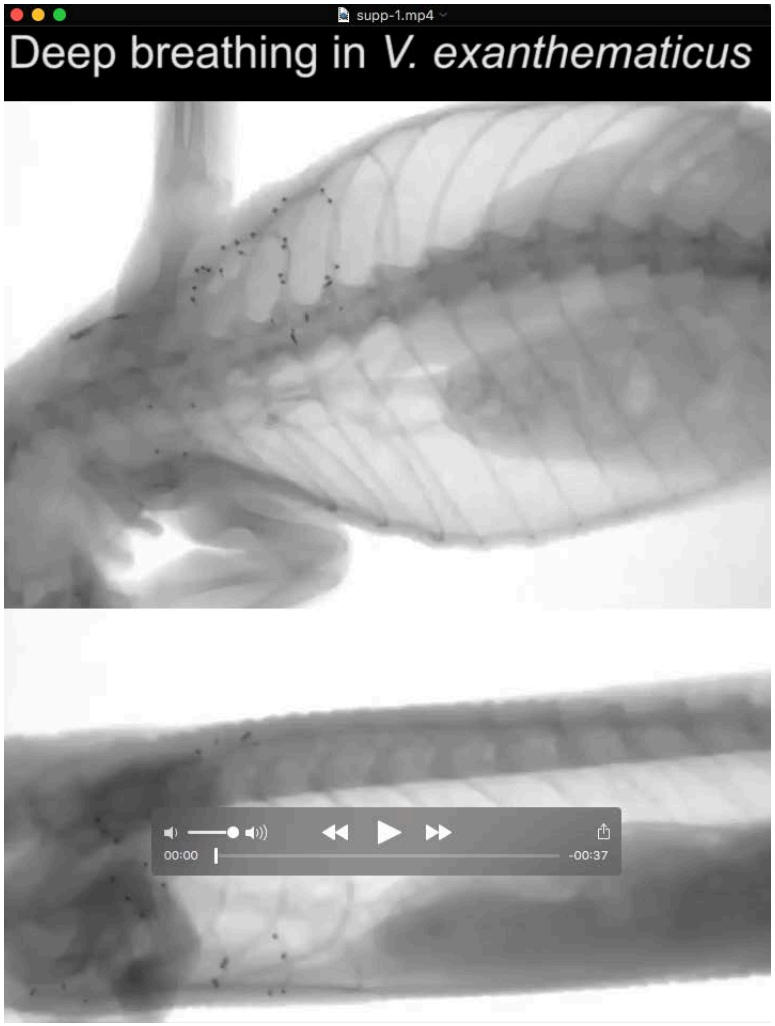

Movie S1 – Biplanar x-ray video of lung ventilation in the savannah monitor (*Varanus exanthematicus*) savannah02. The animal is breathing deeply after treadmill locomotion. Lateral view (left) and dorsal view (right).

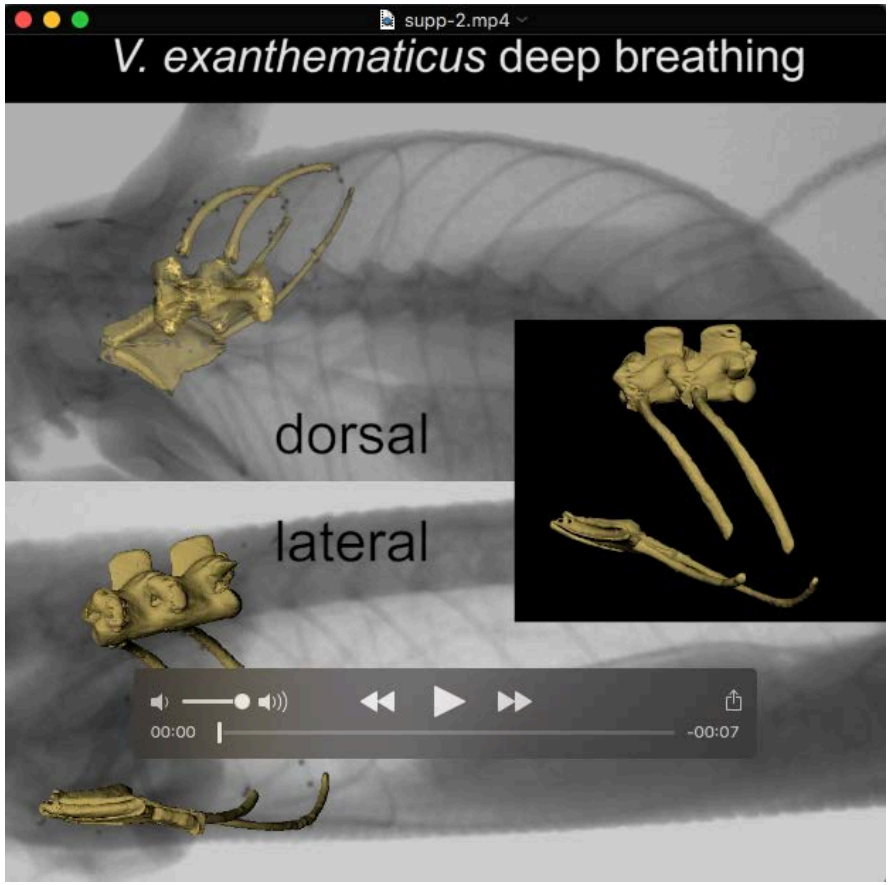

Movie S2 – XROMM animation of the first and second vertebral and sternal ribs during typical deep breathing in the savannah monitor (*Varanus exanthematicus*) savannah02 superimposed upon biplanar x-ray video and the same XROMM animation alone (inset).

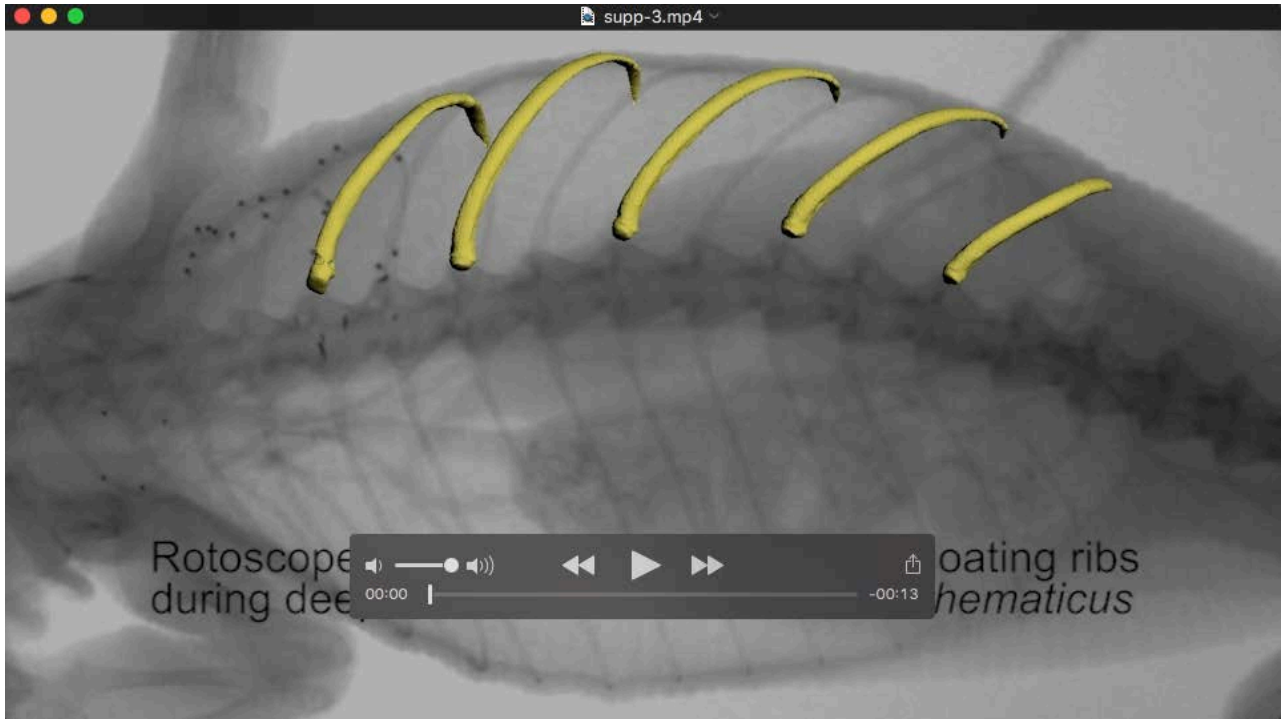

Movie S3 – XROMM animation of the third vertebral and second, fourth, sixth, and eighth floating ribs during deep breathing in the savannah monitor *(Varanus exanthematicus*), savannah02. Bones were animated using Scientific Rotoscoping.

Journal of Experimental Biology • Supplementary information